

Efficient Design of Compact H-plane Rectangular Waveguide Band-Pass Filters with Integrated Coaxial Excitation

A. A. San-Blas^{a,*}, A. Coves^a, A. Vidal^b, V. E. Boria^b

^a*Departamento de Ingeniería de Comunicaciones-I3E, Universidad Miguel Hernández de Elche, Avenida de la Universidad s/n, E-03202 Elche (Spain)*

^b*Departamento de Comunicaciones, Universidad Politécnica de Valencia, Valencia (Spain)*

Abstract

In this work, an efficient procedure for the design of compact H-plane rectangular waveguide band-pass filters including an integrated coaxial excitation is presented. In contrast to classical H-plane filters, where additional input/output boxed cavities are needed to implement the coaxial excitation of the component that usually results in bulky designs, a more compact solution is achieved in this contribution by taking advantage of the resonant behavior of the cited additional cavities. The design strategy, which is based on the well-known Aggressive Space Mapping technique, combines a segmentation of the filter with the use of an equivalent circuit model of the component. The efficiency and accuracy of the proposed approach have been successfully validated with the design of a 7-pole Chebyshev band-pass filter operating in the Ku-band.

Keywords: H-plane filters, band-pass filters, aggressive space mapping, coaxial excitation.

1. Introduction

H-plane rectangular waveguide devices have been widely investigated during the last decades, since these components are frequently used in a wide range of applications for both wireless and satellite communication systems, such as

*Corresponding author

Email address: aasanblas@umh.es (A. A. San-Blas)

5 band-pass filters, multi-port waveguide junctions, diplexers and multiplexers,
 etc. [1, 2, 3, 4, 5]. In particular, the optimized design of H-plane rectangular
 waveguide band-pass filters (also known as inductive waveguide filters) has
 received the attention of many researchers, and different synthesis strategies
 have been proposed over the past years. The cited strategies have been mainly
 10 based either on the obtention of the desired coupling matrix [6, 7, 8], or on the
 derivation of an equivalent circuit model of the waveguide filter [9, 10, 11, 12].
 Space Mapping techniques [13, 14] have also been widely employed for designing
 inductive waveguide filters including rounded corners (in order to account for
 manufacturing inaccuracies), both in the resonators and in the coupling win-
 15 dows [15, 16, 17], and also for filter tuning [18]. Furthermore, H-plane band-pass
 filters are usually fed using a coaxial excitation, especially when the designed
 filter needs to be connected to other components of the system. However, to the
 best of our knowledge, little work has been reported so far for the efficient de-
 sign of classical H-plane rectangular waveguide filters with an integrated coaxial
 20 excitation [19, 20].

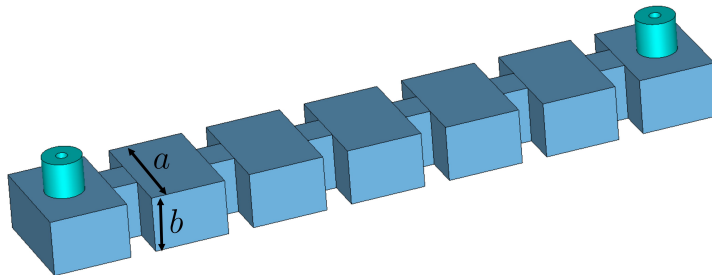


Figure 1: Classical topology of a 5-pole H-plane rectangular waveguide band-pass filter
 with integrated coaxial excitation (the component can be re-designed as a compact
 7-pole band-pass filter).

In this context, therefore, this work focuses on the efficient design of H-plane
 rectangular waveguide band-pass filters including a coaxial excitation, with the
 aim of obtaining a compact final design suitable for next generation commu-
 nication systems based on satellite constellations. The classical topology of a

25 5-pole H-plane band-pass filter excited with coaxial probes is shown in Fig. 1. Note that the filter is composed of the cascade connection of rectangular resonators (of transverse dimensions $a \times b$) and full-height rectangular coupling windows, and also additional input/output rectangular waveguide sections that need to be inserted in the component in order to implement the coaxial excitation. However, this classical topology usually results in a bulky design that could not meet the physical requirements of some applications. With the aim of overcoming this drawback and achieving a more compact solution, we prove in this work that the first and last rectangular sections of the filter in Fig. 1 (i.e., the sections including the coaxial probes that, typically, are just used to implement the input/output couplings) can be properly designed to present, as well, a resonant behavior, thus obtaining a band-pass filter with an increased order. In fact, by following the design procedure presented in this work, the classical fifth-order filter depicted in Fig. 1 could be re-designed as a compact 7-pole band-pass filter, thus increasing the response selectivity without increasing the total insertion losses.

The design procedure that we propose is based on the Space Mapping technique, which was initially presented in [13]. Space Mapping and, particularly, Aggressive Space Mapping (ASM) [14] are powerful optimization techniques that make use of two simulation spaces: a fast and low-accuracy model (the so-called coarse model), and a precise but time-consuming one (known as fine model). The key of these methods is that most simulations of the design process are performed in the coarse model, while the fine model is only used as a reference at the final step of the procedure, thus resulting in a very efficient technique from a computational point of view. In our particular case, the electromagnetic simulations for the coarse model will be performed using the commercial software FEST3D, by choosing a set of simulation parameters that provide us with low-accuracy results but very efficiently. On the other hand, the high-precision simulations needed by the fine model will employ a commercial tool based on the finite-element method (Ansys HFSS).

55 The design method that we present is based on a strategy that combines

a segmentation of the filter (in order to divide the design process into simpler stages with a reduced number of variables to be optimized), with the use of an equivalent circuit model of the filter (based on ideal inverters and distributed elements) that provide us with the desired target performance in each stage of the design process. The objective is to synthesize the dimensions of the structure considered in each stage, in such a way that its full-wave response matches with the response obtained from the corresponding ideal equivalent network. Furthermore, the dimensions obtained at the end of each step of the process will be used as the starting point of the next stage. The approach that we propose has been successfully validated with the full design of a seventh-order Chebyshev band-pass filter operating in the Ku-band ($f_0 = 16$ GHz), with a pass-band return loss of 20 dB and a bandwidth of 300 MHz.

This article is organized as follows. First of all, Section 2 deals with the equivalent circuit model of the filter, while Section 3 discusses the synthesis of the initial dimensions of the coupling windows. Next, a systematic procedure for the efficient design of the filter is presented in Section 4 and, finally, Section 5 details the implementation of the Space Mapping technique, and the characteristics of the final designed filter. Section 6 summarizes the main results obtained in this contribution.

2. Equivalent circuit model of the band-pass filter

The specifications of the H-plane band-pass filter to be designed are as follows. The objective is to design a compact 7-pole Chebyshev band-pass filter (whose topology is represented in Fig. 1), with 20 dB of return loss, centred at $f_0 = 16$ GHz, and considering a bandwidth of 300 MHz. The filter will be implemented in the standard WR-62 rectangular waveguide ($a = 15.7988$ mm, $b = a/2$), and the input and output ports of the component will be 50Ω commercial coaxial connectors ($r_{out} = 2.7456$ mm, $r_{in} = 0.82$ mm, and $\epsilon_r = 2.1$).

Fig. 2 shows the equivalent circuit model of the 7-pole waveguide filter in Fig. 1. This ideal equivalent network is based on impedance inverters and

85 transmission lines of length $\lambda_{g0}/2 = 11.634$ mm, where λ_{g0} represents the guide wavelength of the fundamental mode TE_{10} of the WR-62 waveguide evaluated at f_0 . It is also worth noting that the filter is symmetrical, and that the characteristic impedance and propagation constant of the transmission lines used in Fig. 2 are also referred to the fundamental mode of the rectangular waveguide. Besides, the normalized values K_{ij} of the ideal impedance inverters can be calculated following the well-known analytical expressions found in [21]. The obtained ideal response of the filter is shown in Fig. 3.

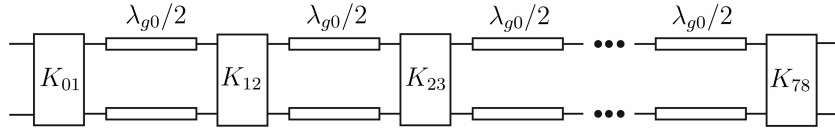


Figure 2: Equivalent circuit model of the seventh-order waveguide band-pass filter.

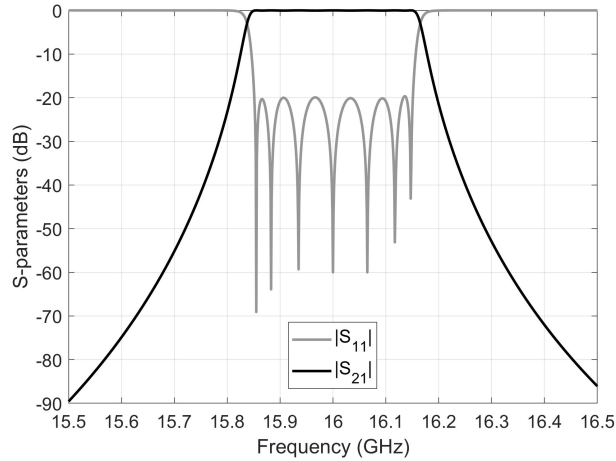


Figure 3: S -parameters of the equivalent circuit model of the filter displayed in Fig. 2.

3. Synthesis of the initial dimensions of the coupling windows

The different resonators of the filter are coupled using full-height rectangular windows (see Fig. 1), whose width can be considered as a key design parameter

since it controls the coupling level between adjacent resonators. Besides, it is worth noting that, in order to guarantee a fast convergence of the design process, it is very important to provide the optimization algorithm with a good starting point. In this context, therefore, this section discusses a procedure to obtain a set of initial dimensions for the width of the coupling windows.

To this aim, we propose to compute the electromagnetic coupling of the structure considered in Fig. 4 as a function of the width a_{ij} of the window (the thickness t of all coupling windows is set at 3.5 mm). Since we are interested in obtaining the resonant frequencies of the structure, note that a very weak coupling (i.e., a very narrow coupling window) is required on the input and output ports of the component. Moreover, the required value of the electromagnetic coupling k_{ij} between the i -th and j -th adjacent resonators can be computed using the equivalent circuit model. In particular, we can state that [21]:

$$k_{ij} = \frac{2K_{ij}}{\pi Z_0} \left(\frac{\lambda_0}{\lambda_{g0}} \right)^2 \quad (1)$$

where K_{ij} represents the value of the inverter of the ideal model (where the relative bandwidth of the frequency response is included), Z_0 is the modal impedance (calculated at f_0) related to the fundamental mode of the WR-62 waveguide, whereas λ_0 and λ_{g0} are, respectively, the free-space and waveguide wavelengths calculated both at f_0 .

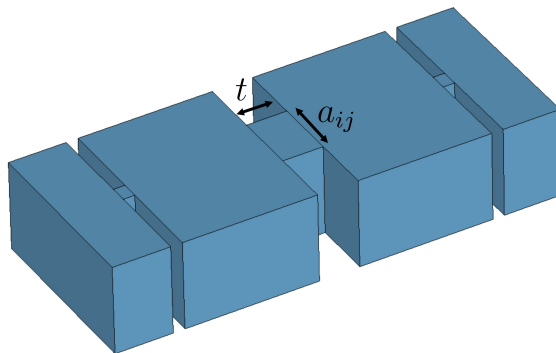


Figure 4: Component considered to determine the initial width a_{ij} of the coupling window that connects the i -th and j -th adjacent resonators.

The parametric curve that relates the electromagnetic coupling with the
 115 width of the coupling windows is shown in Fig. 5. According to eq. (1), the re-
 quired electromagnetic couplings values between resonators are $k_{12} = 1.5569 \cdot 10^{-2}$,
 $k_{23} = 1.1228 \cdot 10^{-2}$, and $k_{34} = 1.0569 \cdot 10^{-2}$ (note that the filter is symmetrical, so
 only the couplings for one half of the filter have been considered). At the sight
 of the results presented in Fig. 5, the following initial dimensions for the widths
 120 of the corresponding coupling windows can be deduced (a lineal interpolation
 has been employed): $a_{12} = 5.47$ mm, $a_{23} = 5.08$ mm, and $a_{34} = 5.01$ mm.

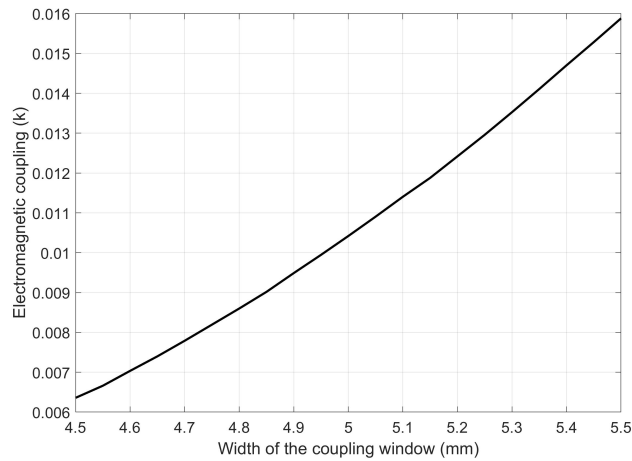


Figure 5: Electromagnetic coupling of the structure of Fig. 4 as a function of the width of the coupling window.

4. Systematic design of the filter using a step-by-step procedure

Next, we discuss the procedure used to design the filter using a step-by-step
 strategy. The design process is segmented into simpler stages in order to reduce
 125 the number of variables to be optimized in each step.

4.1. First stage

In the first stage of the design process, only one rectangular cavity fed by a
 coaxial probe is considered. Furthermore, with the aim of obtaining a compact

design, this first cavity will not only implement the input coupling (as it usually
 130 does in a classical topology), but it will also present a resonant behavior. The
 geometry of the waveguide component considered in this stage is shown in Fig. 6
 (left), where it is worth noting that there is only one access port in the structure
 implemented in coaxial waveguide. The length l_{R1} of the resonator is initially
 set at $\lambda_{g0}/2 = 11.634$ mm, the offset d of the coaxial probe is firstly chosen as
 135 $\lambda_{g0}/4 = 5.817$ mm, while the length l_p of the probe is set at 1.0 mm. On the
 other hand, we show in Fig. 6 (right) the equivalent circuit of the waveguide
 component.

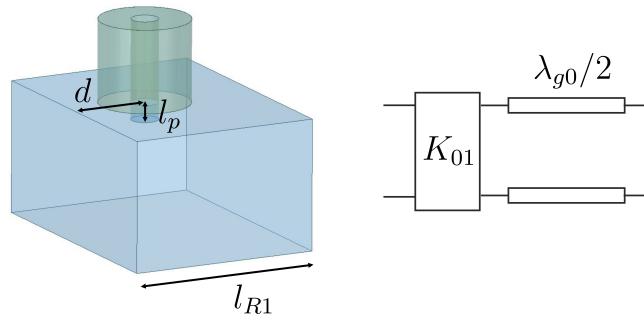


Figure 6: Waveguide component (left) and its equivalent circuit (right) considered in the first stage of the design process.

Next, we are interested in obtaining the group delay of the parameter S_{11}
 of the equivalent circuit model, in order to use this response as a reference
 140 curve. Afterwards, the electrical response of the waveguide component will be
 optimized (using FEST3D) considering the group delay of the equivalent circuit
 model as the target response. The dimensions to be optimized in this stage are
 d , l_p , and l_{R1} (see Fig. 6).

Fig. 7 shows the result of the optimization, where an excellent agreement
 145 between the full-wave response and the target curve is observed. The final
 dimensions of the optimized structure are as follows: $d = 4.603$ mm, $l_p = 1.024$
 mm, and $l_{R1} = 11.481$ mm.

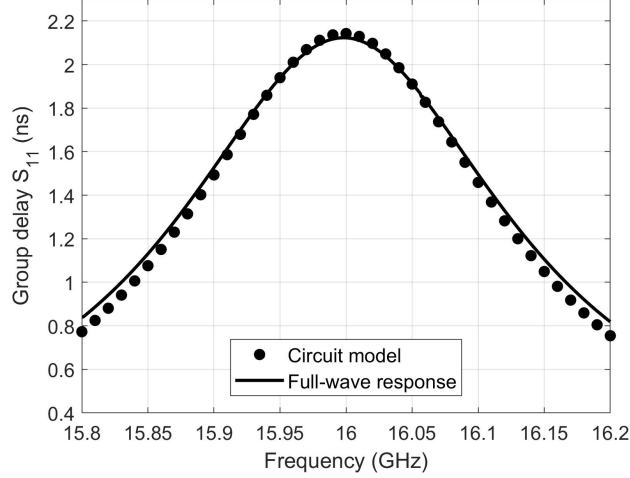


Figure 7: Electrical response of the component of Fig. 6 (left) compared to the ideal response.

4.2. Second stage

In the second stage of the design process, a new resonator is added to the
 150 waveguide component, as shown in Fig. 8 (top). Regarding its equivalent cir-
 cuit model, we have added the inverter K_{12} and a new transmission line, as
 represented in Fig. 8 (bottom). The dimensions to be optimized in this step
 are the variables we optimized in the last stage (d , l_p and l_{R1}), together with
 a_{12} and l_{R2} . According to the results obtained in Section 3, the width a_{12} of
 155 the coupling window is initially set at 5.47 mm, while the length of the second
 resonator is firstly chosen as $l_{R2} = \lambda_{g0}/2$.

As we did in the previous stage, the objective is to optimize the dimensions
 of the waveguide component in order to get an electrical response (in terms of
 the group delay of the S_{11} parameter) as close as possible to the circuit model
 160 response. The results of the optimization are displayed in Fig. 9, where a very
 good agreement is again observed between both types of responses. Finally, the
 optimized dimensions of the structure are (all in mm): $a_{12} = 5.309$, $d = 5.041$,
 $l_p = 0.961$, $l_{R1} = 10.842$, and $l_{R2} = 10.964$.

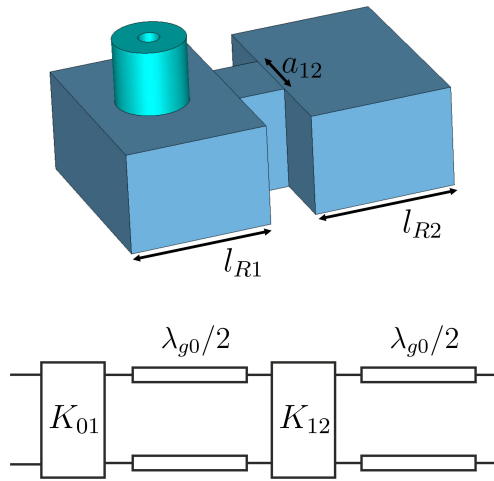


Figure 8: Waveguide component (top) and its equivalent circuit (bottom) considered in the second stage of the design process.

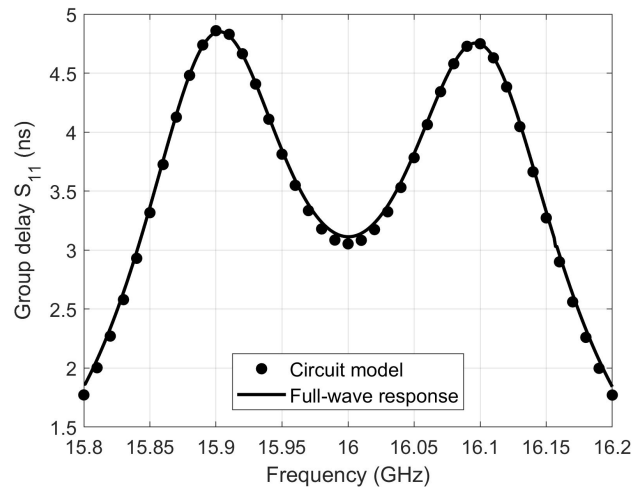


Figure 9: Electrical response of the component of Fig. 8 (top) compared to the ideal response.

4.3. Third and fourth stages

165 In the third and fourth stages of the design process, new resonators are progressively added. For instance, Fig. 10 shows the waveguide component

considered in the fourth stage, as well as its equivalent circuit model. The dimensions to be optimized in these stages are the widths of the coupling windows and the lengths of the resonators (see Fig. 10 for the case of the fourth step), together with the variables d and l_p related to the coaxial excitation (see Fig. 6). Moreover, the lengths of the new resonators added in each step are initially set at $\lambda_{g0}/2$, and the widths of the new added coupling windows are set according to the values synthesized in Section 3. The results of the optimization of the third and fourth stages are shown in Fig. 11 and Fig. 12, respectively, where an excellent agreement is again obtained between the responses of the considered waveguide structures and their ideal equivalent circuits.

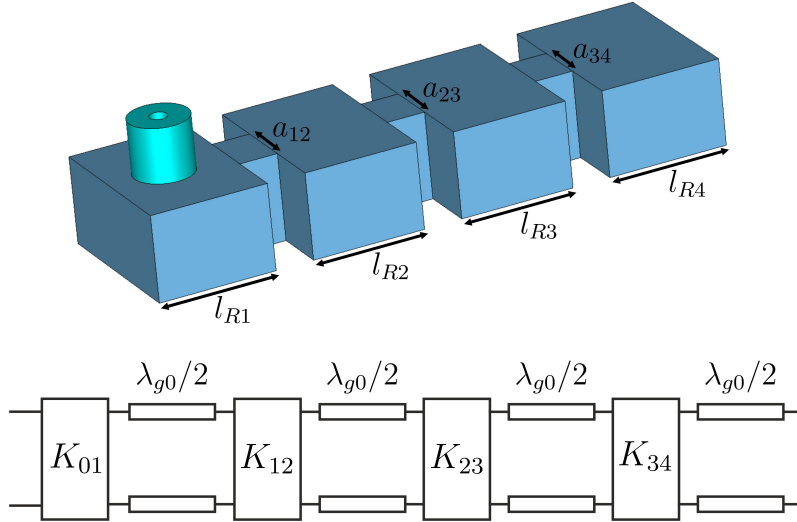


Figure 10: Waveguide component (top) and its equivalent circuit (bottom) considered in the fourth stage of the design process.

Finally, Table 1 collects the obtained values for the dimensions optimized in the fourth stage of the design process. It is worth mentioning that the optimized dimensions obtained for the widths of the coupling windows at the end of the fourth stage are very close to the initial values found in Section 3.

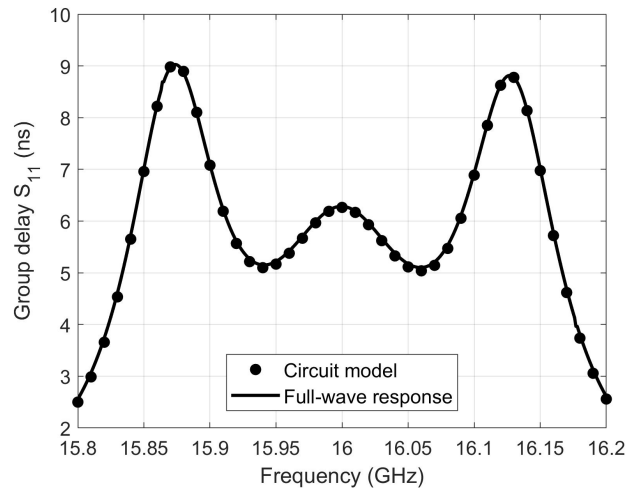


Figure 11: Electrical response obtained after the optimization performed in the third stage of the design process.

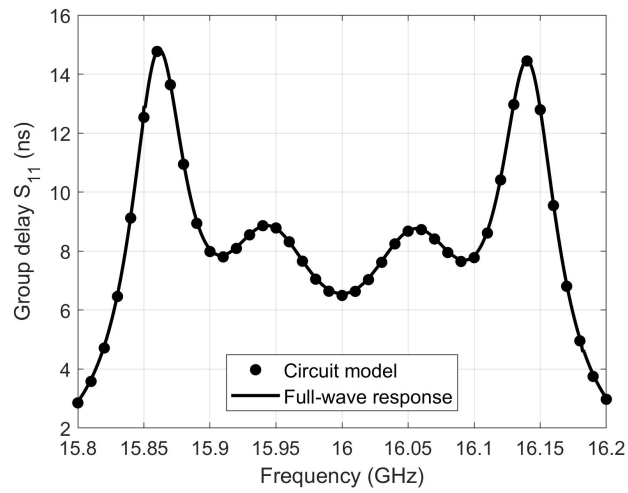


Figure 12: Electrical response obtained after the optimization performed in the fourth stage of the design process.

Table 1: Optimized dimensions of the component shown in Fig. 10.

<i>Dimension</i>	a_{12}	a_{23}	a_{34}	d	l_p	l_{R1}	l_{R2}	l_{R3}	l_{R4}
<i>Value (mm)</i>	5.309	4.971	4.907	5.079	0.952	10.846	10.391	10.503	11.073

4.4. Final stage: design of the complete filter

At this point of the design process, we have completed the synthesis of one half of the filter, since the component is symmetrical. Therefore, the optimization of the whole filter, whose geometry is shown in Fig. 1, is addressed next. We first proceed to calculate the electrical response of the complete filter using the optimized dimensions derived in the previous stage (see Table 1). Fig. 13 shows the obtained S -parameters, after manually adjusting the length l_{R4} of the fourth resonator to take into account the loading effect of the coupling window present at its right side when the whole filter is assembled. To do this, we first calculate $\alpha = \lambda_{g0}/2 - l_{R4}$, in order to estimate the loading effect of the coupling window located at the left side of the fourth resonator in Fig. 10, after completing the fourth stage of the design process. Next, considering the symmetry of the component, we update the length of the cited fourth resonator as follows: $l_{R4,\text{new}} = l_{R4} - \alpha$.

At the sight of the results presented in Fig. 13, it is worth emphasizing that a very good starting point has been obtained, as the pass-band of the filter is very well defined and the seven poles of the electrical response are perfectly visible. However, in order to recover the ideal response of the filter (see Fig. 3), a final optimization is needed. In this last optimization, the target curve is the magnitude of the S_{11} parameter of the ideal network (see Fig. 3), while the dimensions to be optimized are those shown in Table 1.

The results of the optimization are displayed in Fig. 14, where an excellent agreement between the full-wave and the ideal responses of the filter is observed. Finally, the dimensions of the designed H-plane filter are collected in Table 2,

205 where it is worth noting that the obtained final values are very close to those obtained in the fourth stage of the design process (see Table 1), with the exception of l_{R4} , as we discussed before. As a consequence, the design procedure presented in this work provides a significantly enhanced efficiency from a computational point of view.

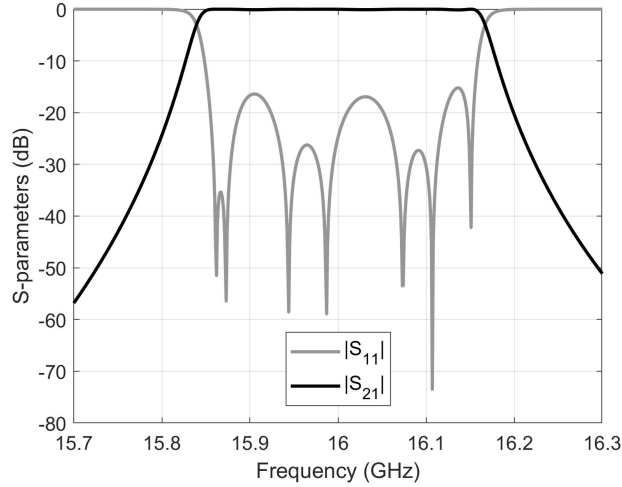


Figure 13: S -parameters of the H-plane filter before the final optimization.

Table 2: Final dimensions of the designed H-plane filter.

<i>Dimension</i>	a_{12}	a_{23}	a_{34}	d	l_p	l_{R1}	l_{R2}	l_{R3}	l_{R4}
<i>Value (mm)</i>	5.304	4.972	4.909	5.128	0.940	10.849	10.390	10.500	10.517

210 5. Implementation of the Space Mapping technique

The design process presented in the previous sections has been performed using FEST3D by choosing a set of simulation parameters that provide us with low-accuracy results. Therefore, the final dimensions obtained in Table 2 are

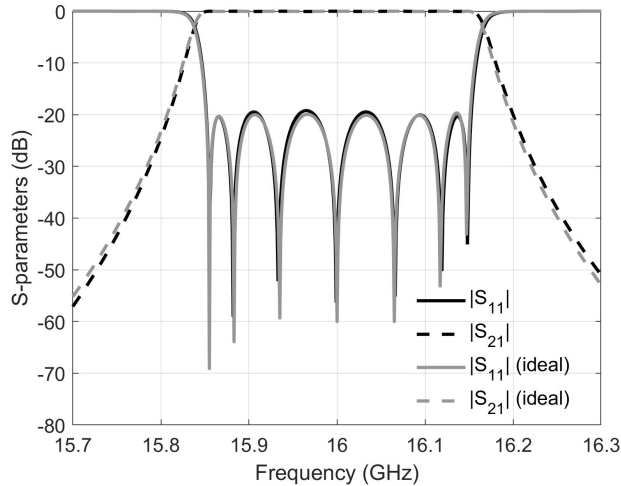


Figure 14: S -parameters of the H-plane filter after the final optimization.

not accurate enough for manufacturing the waveguide component. In this section, the well-known Aggressive Space Mapping (ASM) technique [14] is implemented, with the aim of obtaining accurate dimensions that could be employed to manufacture the band-pass filter. ASM makes use of two different simulation spaces: a fast and low-accuracy model (coarse model), and a precise but time-consuming one (fine model). In the previous sections, all the optimizations have been carried out in the coarse space, thus achieving a final low-accuracy design using low CPU resources (in terms of both time and memory).

Next, we implement the ASM technique, using the commercial software Ansys HFSS for performing the simulations in the high-accuracy (or fine) space. The results are shown in Fig. 15, where we can observe that, with only four iterations, the same electrical response (coarse space response) of the filter designed in Section 4.4 has been recovered, thus fully validating both the accuracy of the results and the proposed design procedure.

The final dimensions of the filter are reported in Table 3. It is worth noting that the obtained final dimensions are very close to the corresponding values of the filter designed in the coarse space (see Table 2), and this explains why ASM

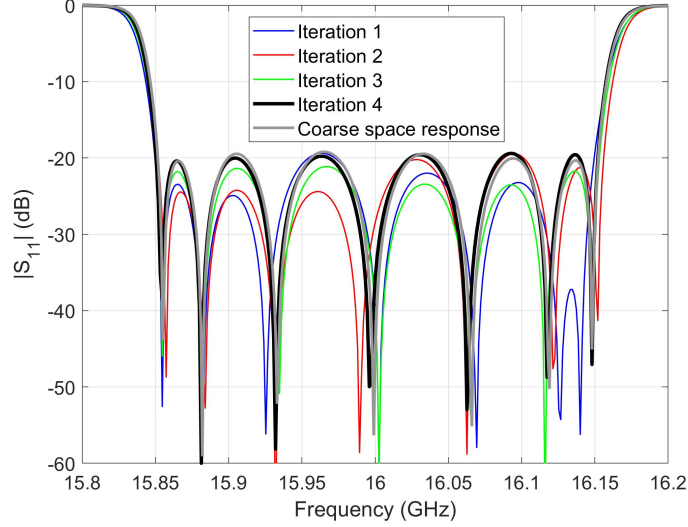


Figure 15: Implementation of the ASM technique to recover the electrical response of the filter designed in the coarse space. The simulations have been performed using Ansys HFSS.

has reached convergent results with a low number of iterations.

Table 3: Dimensions of the H-plane filter designed in the high-accuracy space.

<i>Dimension</i>	a_{12}	a_{23}	a_{34}	d	l_p	l_{R1}	l_{R2}	l_{R3}	l_{R4}
<i>Value (mm)</i>	5.291	4.962	4.900	5.247	0.783	10.903	10.371	10.482	10.499

Finally, with the aim of evaluating the degree of compactness achieved by our filter topology, we have also designed (following the same design procedure) a classical 7-pole H-plane band-pass filter with an integrated coaxial excitation (see Fig. 16), which features exactly the same electrical performance than the designed compact filter, but using an increased number of boxed cavities. According to the dimensions presented in Table 3, the total length of the compact filter is 95.011 mm, while the length of the classical solution increases up to

125.527 mm (the thickness of the coupling windows is the same we used for the
compact design). Therefore, the new designed topology is 24.3% more compact
than the classical one.

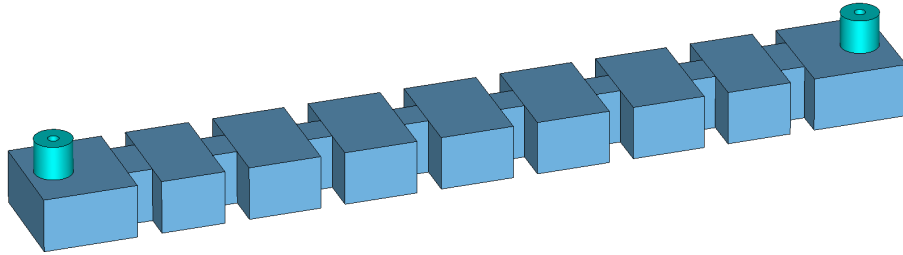


Figure 16: Topology of a classical seventh-order H-plane band-pass filter including a coaxial excitation.

6. Conclusion

In this contribution, a technique for the efficient design of compact H-plane rectangular waveguide band-pass filters with an integrated coaxial excitation has been discussed in detail. The proposed design strategy is based on a step-by-step procedure, where the different resonators of the filter have been progressively added one after the other. Furthermore, the electrical response of the equivalent circuit network of the waveguide component considered in each stage of the design process, has been used as a target curve to optimize the dimensions of the filter. The key novelty of this work lies in the fact that, unlike classical H-plane band-pass filters, the input/output waveguide sections used to implement the coaxial excitation, not only provided us with the desired input/output coupling, but also they have been designed to present a resonant behavior, thus increasing the order of the designed filter (enhancing the response selectivity) and achieving a more compact solution. Moreover, the well-known Aggressive Space Mapping technique has been employed to obtain a set of accurate dimensions that could be used for manufacturing purposes. The presented technique has been validated with the complete design of a seventh-order band-pass filter operating in the Ku-band.

260 **Funding**

This research was supported by the Ministerio de Ciencia e Innovación, Spanish Government, under R&D Projects PID2019-103982RB-C41 and PID2019-103982RB-C43.

References

- 265 [1] A. A. San-Blas, V. E. Boria, B. Gimeno, S. Cogollos, Design of compensated multiport waveguide junctions considering mechanization effects, *AEU - International Journal of Electronics and Communications* 69 (1) (2015) 328–331.
- [2] F. Teberio, I. Arregui, M. Guglielmi, A. Gómez-Torrent, P. Soto, M. A. G. Laso, V. E. Boria, Compact broadband waveguide diplexer for satellite
270 applications, in: 2016 IEEE MTT-S International Microwave Symposium (IMS), 2016, pp. 1–4.
- [3] A. P. Abenza, M. Martínez-Mendoza, F. D. Quesada-Pereira, A. Álvarez-Melcón, Design of manifold multiplexers in all-inductive dual-mode rectangular waveguide technology using the coupling matrix formalism, *Radio
275 Science* 51 (7) (2016) 1065–1080.
- [4] H. Wang, W. Hu, R. Liu, L. Si, J. Yin, T. Dong, A design of 300 GHz waveguide bandpass filter with H-plane offset inductive window, in: 2016 IEEE 9th UK-Europe-China Workshop on Millimetre Waves and Terahertz
280 Technologies (UCMMT), 2016, pp. 189–191.
- [5] J. Champion, O. Glubokov, A. Gómez, A. Krivovitca, U. Shah, L. Bolander, Y. Li, J. Oberhammer, An ultra low-loss silicon-micromachined waveguide filter for D-band telecommunication applications, in: 2018 IEEE/MTT-S International Microwave Symposium - IMS, 2018, pp. 583–586.
- 285 [6] M. Martínez-Mendoza, F. J. Pérez-Soler, J. S. Gómez-Díaz, F. Quesada-Pereira, A. Álvarez-Melcón, R. J. Cameron, Enhanced topology for the

design of bandpass elliptic filters employing inductive windows and dielectric objects, in: 2008 IEEE MTT-S International Microwave Symposium Digest, 2008, pp. 635–638.

- 290 [7] M. Martínez-Mendoza, D. Canete-Rebenaque, A. Álvarez-Melcón, Synthesis and design of a dual-band dual-mode filter in all inductive waveguide technology, in: 2014 44th European Microwave Conference, 2014, pp. 612–615.
- [8] M. M. Mendoza, D. Martínez, D. C. Rebenaque, A. Álvarez-Melcón, Enhanced topologies for the design of dual-mode filters using inductive waveguide structures, *Radio Science* 50 (1) (2015) 66–77.
- 295 [9] M. Guglielmi, Simple CAD procedure for microwave filters and multiplexers, *IEEE Transactions on Microwave Theory and Techniques* 42 (7) (1994) 1347–1352.
- [10] P. Soto, E. Tarín, V. E. Boria, C. Vicente, J. Gil, B. Gimeno, Accurate synthesis and design of wideband and inhomogeneous inductive waveguide filters, *IEEE Transactions on Microwave Theory and Techniques* 58 (8) (2010) 2220–2230.
- 300 [11] A. A. San-Blas, J. C. Melgarejo, V. E. Boria, M. Guglielmi, Novel solution for the coaxial excitation of inductive rectangular waveguide filters, in: 2018 48th European Microwave Conference (EuMC), 2018, pp. 89–92.
- [12] A. A. San-Blas, M. Guglielmi, J. C. Melgarejo, A. Coves, V. E. Boria, Design procedure for bandpass filters based on integrated coaxial and rectangular waveguide resonators, *IEEE Transactions on Microwave Theory and Techniques* 68 (10) (2020) 4390–4404.
- 310 [13] J. W. Bandler, R. M. Biernacki, Shao Hua Chen, P. A. Grobelny, R. H. Hemmers, Space mapping technique for electromagnetic optimization, *IEEE Transactions on Microwave Theory and Techniques* 42 (12) (1994) 2536–2544.

- 315 [14] J. W. Bandler, R. M. Biernacki, Shao Hua Chen, R. H. Hemmers, K. Madsen, Electromagnetic optimization exploiting aggressive space mapping, *IEEE Transactions on Microwave Theory and Techniques* 43 (12) (1995) 2874–2882.
- [15] J. V. Morro, P. S. Pacheco, H. Esteban, V. E. Boria, C. Bachiller,
320 M. Taroncher, S. Cogollos, B. Gimeno, Fast automated design of waveguide filters using aggressive space mapping with a new segmentation strategy and a hybrid optimization algorithm, *IEEE Transactions on Microwave Theory and Techniques* 53 (4) (2005) 1130–1142.
- [16] E. Díaz-Caballero, J. V. Morro, A. Belenguer, H. Esteban, V. E. Boria,
325 CAD technique for designing H-plane waveguide filters considering rounded corners, in: *2013 IEEE MTT-S International Microwave Symposium Digest (MTT)*, 2013, pp. 1–3.
- [17] A. Rodríguez, J. V. Morro, J. Selga, M. Sans, J. Ossorio, M. Guglielmi,
330 F. Martín, V. E. Boria, Robust optimization and tuning of microwave filters and artificial transmission lines using aggressive space mapping techniques, in: *2017 IEEE MTT-S International Microwave Symposium (IMS)*, 2017, pp. 1501–1504.
- [18] J. C. Melgarejo, J. Ossorio, S. Cogollos, M. Guglielmi, V. E. Boria, J. W. Bandler, On space mapping techniques for microwave filter tuning, *IEEE Transactions on Microwave Theory and Techniques* 67 (12) (2019) 4860–
335 4870.
- [19] V. E. Boria, G. Gerini, M. Guglielmi, Computer aided design of reentrant coaxial filters including coaxial excitation, in: *1999 IEEE MTT-S International Microwave Symposium Digest (Cat. No.99CH36282)*, Vol. 3, 1999,
340 pp. 1131–1134 vol.3.
- [20] G. Gerini, M. Guglielmi, Full-wave CAD of a rectangular waveguide filter with integrated coaxial excitation, *IEEE Transactions on Microwave Theory and Techniques* 49 (5) (2001) 986–989.

- [21] G. Matthaei, L. Young, E. M. T. Jones, Microwave Filters, Impedance-Matching Networks, and Coupling Structures, Artech House, Norwood, 1980.